Structure and Bonding of Gold Metal Clusters, Colloids, and Nanowires Studied by EXAFS, XANES, and WAXS

Robert E. Benfield* and Didier Grandjean

Centre for Materials Research, School of Physical Sciences, University of Kent, Canterbury CT2 7NR, U.K.

Michael Kröll, Raphael Pugin, Thomas Sawitowski, and Günter Schmid*

Institut für Anorganische Chemie, Universität GH Essen, Universitätsstrasse 5-7, D-45117 Essen, Germany

Received: August 9, 2000; In Final Form: November 28, 2000

The structure and bonding of a series of gold clusters and gold nanomaterials stabilized by ligands or confined within nanoporous alumina have been investigated using EXAFS, XANES, and WAXS. Two gold clusters stabilized by two different ligands, $Au_{55}(PPh_3)_{12}Cl_6$ and $Au_{55}(T_{8-}OSS-SH)_{12}Cl_6$, were confirmed to be of face-centered cubic structure type with metal−metal distances of 2.785 and 2.794 Å, respectively, shorter than in bulk gold. Colloidal gold of 180 Å diameter stabilized by sulfonated phosphine ligands had structural and electronic properties very similar to those of bulk gold but smaller Debye−Waller factors. The cluster $Au_{55}(PPh_3)_{12}Cl_6$ adsorbed into nanoporous alumina membrane was found to retain its integrity inside the membrane but with slightly longer Au−Au bonds due to some aggregation. The same cluster thermally transformed into colloidal gold within the alumina membrane was found to be almost identical structurally and electronically to the bulk. Gold nanowires electrochemically grown within the nanoporous alumina were found to be composed on average of 120 Å diameter crystallites. These have the same structure as the bulk, but with smaller Debye−Waller factors, indicating either a better crystallinity or that the gold atoms are more tightly held than in the bulk. The difference of area method $L_3 - kL_2$ was used to quantify the d orbital occupancy. The two ligand-stabilized Au_{55} clusters both had a smaller value (2.7) than the bulk material (4.1). The nanomaterials inside the membrane also showed smaller $L_3 - kL_2$ values. The geometrical and electronic structures of these gold materials show a very clear pattern of buildup as the number of gold atoms increases from Au_{55} clusters through Au colloids and nanowires to the bulk metal.

Introduction

Nanoscale materials are today of great importance due to their diverse range of electrical and catalytic properties. Ligand-stabilized metal clusters are considered to be model compounds for the catalytic properties of very small metal particles as well as potential basic devices for the ultimate miniaturization in electronics.[1]

The properties of these metal clusters can be expected to be intermediate between those of metals and isolated atoms and may be used to study effects such as the onset of metallic behavior. In comparison to bulk metals, clusters may also have a different structure. There is general experimental and theoretical agreement that cluster materials of some metals, such as gold and platinum, show a lattice contraction compared to the bulk metals. For other metals, the experimental picture is unclear.[2]

The development of cluster electronic structure from the covalent bonding of small molecular clusters toward the delocalized metallic bonding of bulk metals is also the focus of intense interest.[3−5] For future application of supported metal cluster materials in nanoelectronics, ligand-stabilized metal clusters of quantum-dot size are to be synthesized and positioned on surfaces and in confined spaces in a regularly spaced manner.[6]

Of great interest are the supported and insulated one-dimensional "quantum wire" materials derived from metal clusters adsorbed into nanoporous alumina membranes. The pores can be partly or completely filled with ligand-stabilized metal clusters, which can then be thermally decomposed into larger clusters or colloids.[7] The affinity of the cluster for adsorption onto the inner pore surface of the alumina membrane can also be controlled by the type of ligand used. In an alternative method, metal "nanowires" can be grown within the alumina electrochemically.[8] These nanowires are not fully continuous, but are aggregates of crystallites with Coulomb blockades.

Due to a lack of detectable long-range order in this type of cluster material, EXAFS, XANES, and WAXS are particularly well-suited to characterize the geometrical structures and metal−metal distances as well as to give insight into the electronic structures of these nanomaterials. Here we report a study of ligand-stabilized gold clusters and colloids, and gold clusters, colloids, and nanowires within nanoporous alumina. The aims of this study are to characterize the structure and electronic character of these different gold materials, and to determine the influence on them of the support materials. This will achieve a better understanding of the physical properties of the nanomaterials.

Experimental Section

Synthesis. *Clusters and Colloids.* Two 55-atom gold clusters (core diameter of ∼14 Å) stabilized with different ligands were

* To whom correspondence should be addressed. (R.E.B.) Fax.: +44-1227-827558. E-mail: R.E.Benfield@ukc.ac.uk. (G.S.) Fax.: +49-201-1832402. E-mail: guenter.schmid@uni-essen.de.

10.1021/jp0028812 CCC: $20.00
Published on Web 02/17/2001

prepared. The cluster $Au_{55}(PPh_3)_{12}Cl_6$ was synthesized as previously reported.[9] The silsesquioxane-stabilized Au_{55} cluster $Au_{55}(T_8-OSS-SH)_{12}Cl_6$ was synthesized by a ligand exchange reaction using the triphenylphosphane-stabilized Au_{55} cluster and $(cyclopentyl)_7Si_8O_{12}(CH_2)_3SH$ ($T_8-OSS-SH$) as starting materials. Details are described elsewhere.[10] Gold colloids of ~180 Å diameter stabilized by sulfonated phosphine ligands were synthesized as previously reported.[11]

Nanoporous Alumina Membranes. Nanoporous alumina membranes are formed by a well-established procedure.[12−15] High-purity (>99.99%) aluminum plates or foils are electropolished in a mixture of 60% w/w phosphoric acid and 40% w/w sulfuric acid. Polishing takes place at a temperature of about 70 °C using a lead plate as cathode. The potential applied for polishing is 15 V. Depending on the pore size, two different electrolytes are used for anodizing the aluminum afterward. For pore diameters smaller than 30 nm 10% w/w sulfuric acid is used; for larger pores we use a 4% w/w oxalic acid solution. Anodization takes place at 0 °C again using a lead plate as cathode. The pore diameter depends on the anodizing voltage applied (1.0−1.5 nm V^{-1}). The membrane used in this study was grown at 40 V and presented an average pore diameter (determined by TEM and AFM) of ca. 56 nm. A more general characterization of these membranes in terms of pore size distribution and organization is currently under investigation using SAXS.[16]

After anodizing there is a compact oxide layer between the porous membrane and the aluminum. For the cluster filling experiments this barrier layer has to be removed. Since the thickness of the barrier layer also depends on the anodizing voltage, it is reduced stepwise at the end of the anodizing procedure. When the plate is dipped in a dilute acid afterward, the barrier layer is removed nearly completely. The acid reaches the aluminum, resulting in a hydrogen evolution. The hydrogen lifts the porous membrane and thus separates the membrane from the aluminum.

Metal-Filled Membranes. The clusters can be filled into the pores by vacuum induction, electrophoretically, or by a capillary-dipping procedure. The gold clusters were then thermally decomposed into colloids within the alumina.[7]

An alternative method to produce gold nanowires is to use an ac plating procedure.[8] A solution of 1 g/L $HAuCl_4$ in water is used as electrolyte. The aluminum and the barrier layer are left intact in this case. The aluminum serves as an electrode during the electroplating. Graphite is used as counter electrode. An ac voltage of 9 V is now applied for 30 min. The barrier layer serves as a rectifier (valve metal oxide), allowing the cathodic half-cycle of the current to plate the metal inside the pores and reducing the anodic half-cycle to an extent that is not high enough to reoxidize the metal inside the pores completely, but still prevents the system from being polarized (which would be the case when using dc instead of ac). After the gold is plated the aluminum is dissolved by a 10% solution of Br_2 in methanol.

X-ray Measurements. *EXAFS*. X-ray absorption data were collected on beamline 9.2 (CLRC Daresbury Laboratory, U.K.), operating under beam conditions of 2 GeV and 200 mA using a Si(220) double-crystal monochromator. EXAFS signals were measured at the Au L_3 edge (11 918.7 eV).

Samples of $Au_{55}(PPh_3)_{12}Cl_6$, $Au_{55}(T_8-OSS-SH)_{12}Cl_6$, and gold colloids of 180 Å diameter stabilized by sulfonated phosphine ligands were ground with boron nitride and pressed into pellets, producing an edge jump between 0.2 and 1 in transmission mode. Alumina membrane samples (40 V) filled with $Au_{55}(PPh_3)_{12}Cl_6$ and Au_{55} clusters thermally decomposed into gold colloids were studied as membrane films, stacked several layers thick to obtain a suitable edge jump in fluorescence mode. Alumina membranes (40 V) filled with electrochemically grown gold nanowires were ground with boron nitride and pressed into pellets, producing a suitable edge jump in fluorescence mode. Gold metal foil of 5 μm thickness was used as a reference standard. Ionization chambers were filled with standard Ar/Kr mixtures. Measurements in fluorescence mode were made using a 13-channel signal detector, with several datasets summed to improve signal/noise ratios. Exact calibration of the X-ray energy for detailed comparison of the XANES features was achieved by simultaneously recording a Au foil spectrum in the monitor position with a third ionization chamber. In all cases the monochromator was detuned on its rocking curve to approximately half the maximum transmitted X-ray intensity to reduce the harmonic content of the beam at a minimum level.

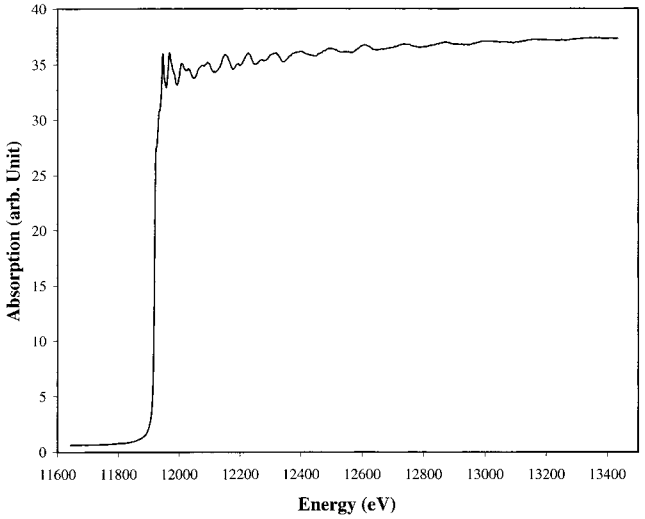

Figure 1. Raw Au L_3 edge X-ray absorption spectrum of the gold nanowire sample in fluorescence mode.

The spectra were recorded at both 300 and 80 K by cooling the samples with a coldfinger liquid nitrogen cryostat. Au L_3 edge transmission and fluorescence EXAFS were collected up to $k = 20$ Å^{-1}. The high quality of the EXAFS data is shown by the example of the electrochemically grown gold nanowires in Figure 1. XANES spectra were also recorded at the Au L_2 edge (13733.6 eV).

WAXS. WAXS data were collected on beamline ID01 (ESRF Grenoble, France) operating under beam conditions of 6 GeV, 90 mA, and 16 Bunch mode using an X-ray energy of 8.089 keV, corresponding to a wavelength of 1.5315 Å. $Au_{55}(PPh_3)_{12}Cl_6$ and $Au_{55}(T_8-OSS-SH)_{12}Cl_6$ were studied as powders in a capillary tube; the 40 V alumina membranes filled with electrochemically grown gold nanowires were mounted as films in the X-ray beam. WAXS was recorded at ambient temperature using 2θ scanning mode to an angle of 150° using typically five data points per degree with a count time of 1 s.

Data Analysis. *EXAFS*. Data reduction of experimental X-ray absorption spectra was performed using the program EXBROOK.[17] Preedge background subtraction and normalization were carried out by fitting a linear polynomial to the preedge region and cubic splines to the postedge region of the absorption spectrum. A smooth atomic background was obtained. EXAFS refinements were performed with the EXCURV98 package.[17] Phase shifts and backscattering factors were calculated ab initio using Hedin−Lundqvist potentials.

TABLE 1: Summary of Structural Results of Au L_3 Edge EXAFS Refinements of Bulk Gold and the Series of Gold Nanomaterials[a]

	bulk gold	gold nanowire in Al_2O_3	$Au_{55}(T_8$–OSS–$SH)_{12}Cl_6$	$Au_{55}(PPh_3)_{12}Cl_6$	$Au_{55}(PPh_3)_{12}Cl_6$ in Al_2O_3	colloid (thermally grown) in Al_2O_3	colloid (ligand-stabilized)
E_f	−7.7(4)	−8.0(6)	−6.3(7)	−5.7(6)	−9.5(9)	−9.1(6)	−8.6(8)
AFAC	0.8	0.8	0.8	0.8	0.8	0.8	0.8
symm	fcc	fcc			fcc	fcc	fcc
N_1	12	12	6.3 (5)	6.5(4)	7(2) [0.6(1) × 12]	12	8.6(2) [0.72(1) × 12]
a	4.045(3)	4.058(2)			4.016(7)	4.046(3)	4.049(2)
R_1	2.860(4)	2.869(3)	2.794(3)	2.785(3)	2.84(1)	2.861(4)	2.863(3)
A_1	0.0141(2)	0.0073(1)	0.017(1)	0.017(1)	0.016(1)	0.0110(2)	0.00622(2)
A_2	0.022(3)	0.012(1)	S: $N_2 = 0.5(2)$ $R_2 = 2.3(1)$ $A_2 = 0.0095(4)$	P: $N_2 = 0.2(1)$ $R_2 = 2.30(1)$ $A_2 = 0.003(3)$	0.030(9)	0.022(5)	0.009(1)
A_3	0.023(2)	0.011(1)			0.031(5)	0.017(1)	0.009(1)
A_4	0.024(2)	0.017(3)			0.04(1)	0.018(2)	0.015(2)
A_5	0.030(6)	0.02(1)			0.03(3)	0.027(7)	0.016(4)
R factor	25	21.0	29.5	26.9	35.7	26.9	22.6

[a] E_f = contribution of the wave vector of the zero photoelectron relative to the origin of k (eV). AFAC = amplitude reduction due to many-electron processes. N_i = number of atoms in the ith shell. R_i = radial distance of atoms in the ith shell (Å). a = cell parameter (4.0786 Å from ref 18). A_i = Debye−Waller term of the ith shell ($A = 2\sigma^2$ with σ = Debye−Waller factor) (Å^2). R factor in percent. S = sulfur. P = phosphorus.

The data were refined over the full k range without the use of Fourier filtering techniques. Refinements were carried out using k^3 and k^2 weighting. The refined parameters were virtually identical in both cases, although k^2 weighting gave a more equal amplitude to the weighted EXAFS oscillations over the wide range of k values covered by the data.

Contributions from multiple scattering paths become significant when quantitative EXAFS analysis of higher neighboring shells in a structure is desired. Full account of the multiple scattering has therefore been taken in this study. In the face-centered cubic (fcc) structure of bulk Au the three-body configuration paths 0−1−4−0 and 0−1−4−1−0 (including atoms of the first and fourth shells) in collinear arrangement[17] corresponding to scattering paths of 11.46 Å were found to contribute the most significantly to the theoretical $\chi(k)$ function, giving a small peak at ∼5.7 Å, which emphasized the fourth shell. Multiple scattering paths were calculated up to 12 Å. At higher distances the number of scattering paths with equally very small amplitude increases significantly, so quadruple and higher multiple scattering paths were discarded.

Possible asymmetric oscillation effects in the interatomic radial distribution were fully accounted for in the refinements. However, these effects were found to be negligible at 80 K for all the samples.

The fcc structure of bulk gold based on crystallographic data taken from the CDS database[18] was used as a model for the theoretical EXAFS calculations. Except for the Au_{55} clusters, in which nearest-neighbor Au−Au distances dominate due to the small cluster size, the built-in program SYMMETRY[17] was used to generate automatically all the shell parameters (coordination number, distance) corresponding to the fcc structure. In this case, only the cell parameter, the Debye−Waller factors for every shell, E_f (contribution of the wave vector of the zero photoelectron relative to the origin of k), and the AFAC factor (amplitude reduction due to many-electron processes) were used as adjustable parameters in the fitting process, reducing significantly the number of variables in the EXAFS refinements.

In the case of the colloids a weighting factor N_0 applied to all the coordination numbers of the different shells was used. It allowed us to refine a full fcc structure including the full multiple scattering calculation taking into account the lower coordination numbers due to the presence of a great number of surface atoms.

XANES. To obtain a reliable alignment of the XANES spectra, the first derivatives of the raw data from the monitor channel were linearly calibrated and superimposed on each other.

XANES analysis was carried out using the "$L_3 - kL_2$" method.[19] The areas under the first peaks of the L_3 and L_2 spectra were subtracted after normalization of the step to unity.

WAXS. WAXS data were fitted by modeling Gaussian peaks in the program SPECPLOT.[20] The widths of the (111) peaks were related to crystallite size using the Scherrer equation. The fwhm were corrected by subtracting the corresponding fwhm of the gold foil peaks to take account of the resolution limit of the goniometer.

Results and Discussion

EXAFS Analysis. *Results*. Results of the EXAFS structural refinements are summarized in Table 1.

All the EXAFS best fits and the Fourier transform (FT) plots are presented in Figures 2 and 3, respectively. Several structure trials have confirmed that all the samples in this study have a bulklike fcc structure as previously suggested. All the refinements using this structural model (except for the cluster in the alumina membrane) have led to best fit values with R factors in the range of 21−29%.

The FTs of all the samples under investigation are gathered in Figure 4. They can be analyzed according to four different shapes.

The first one corresponds to the bulk gold, the nanowire produced by the ac plating procedure, and the colloid made by heating the clusters inside the pores. They all exhibit the typical FT pattern of the fcc structure. The very good quality of the data allowed the peaks to be very well defined up to at least 7 Å. The first peak for both samples is located at 2.7 Å before phase correction. The peak of the nanowire showed a strong increase in magnitude in comparison to the one belonging to bulk gold.

The second type of FT corresponded to the $Au_{55}(PPh_3)_{12}Cl_6$ and $Au_{55}(T_8-OSS-SH)_{12}Cl_6$ ligand-stabilized clusters featuring only one main peak at 2.6 Å before phase correction with a much smaller intensity than the bulk and nanowire. These peaks are obviously broader and shifted toward smaller R in comparison to the bulk and nanowire. Due to the very small size of these clusters, no other shell beyond the first one could be seen. The inclusion of an extra shell accounting for light atoms (P or

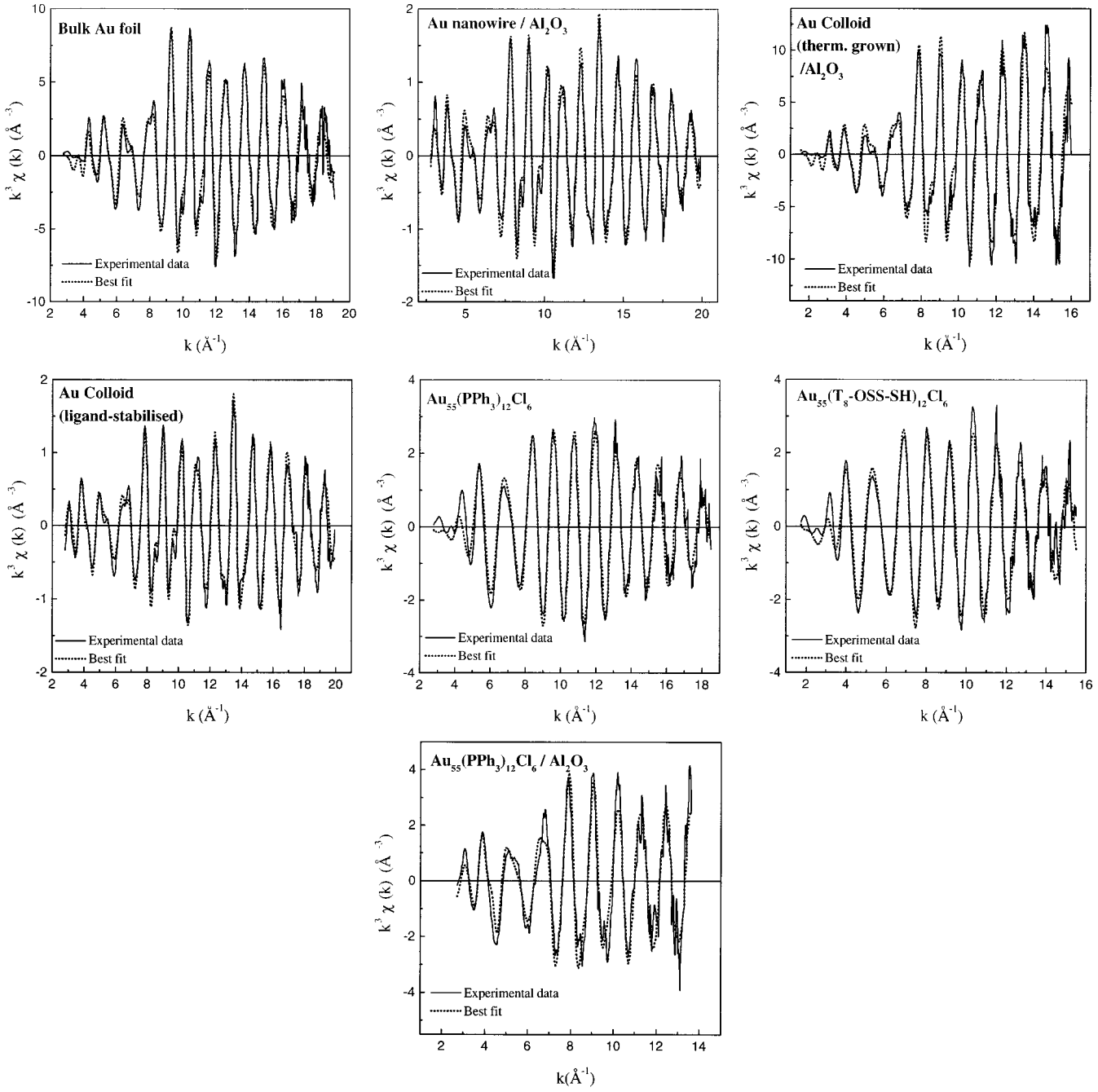

Figure 2. Au L_3 edge EXAFS spectra (after background subtraction, k^3-weighted) of bulk gold and the series of gold nanomaterials. The solid lines are the experimental data, and the dotted lines are the best fits.

S) corresponding to the ligand bonding led to a statistically significant improvement in the refinements.

The third type of FT corresponds to the phosphine-stabilized colloid, which features up to 6 Å almost the same peaks as the bulk series but with a much smaller intensity. Beyond 6 Å no peaks are seen because of the limited size of this colloid.

Finally, the last type is the cluster adsorbed into the alumina membrane whose shape can be viewed as between those of the clusters and the bulk with a much broader main peak at a slightly higher distance (2.65 Å before phase correction) than for the cluster before adsorption.

Discussion. The evolution of the first metal−metal distance (Table 1), which decreases from 2.869 Å for the nanowires and 2.860 Å for the bulk gold and the ligand-stabilized colloid to 2.785 and 2.794 Å for the two ligand-stabilized clusters confirms the contraction of the first coordination shell distance observed previously in the case of the Au_{55} clusters.[3, 21]

The cluster inside the alumina membrane features an intermediate R value at 2.84 Å. This could indicate that some aggregation has occurred and that the Au−Au bond distance could be correlated to some extent with the size of the particle.

The Debye−Waller terms A ($A = 2\sigma^2$, where σ is the Debye−Waller factor) corresponding to the first shell (Table 1) show a great variation according to the type of sample, from 0.0073 Å^2 for the nanowires grown by electroplating to 0.0141 Å^2 for the bulk Au and up to 0.017 Å^2 for the two ligand-stabilized Au_{55} clusters.

The magnitude of the FT peak is inversely related to the Debye−Waller factor, accounting for static and thermal vibrational disorder. In the case of the nanowire sample, the peak

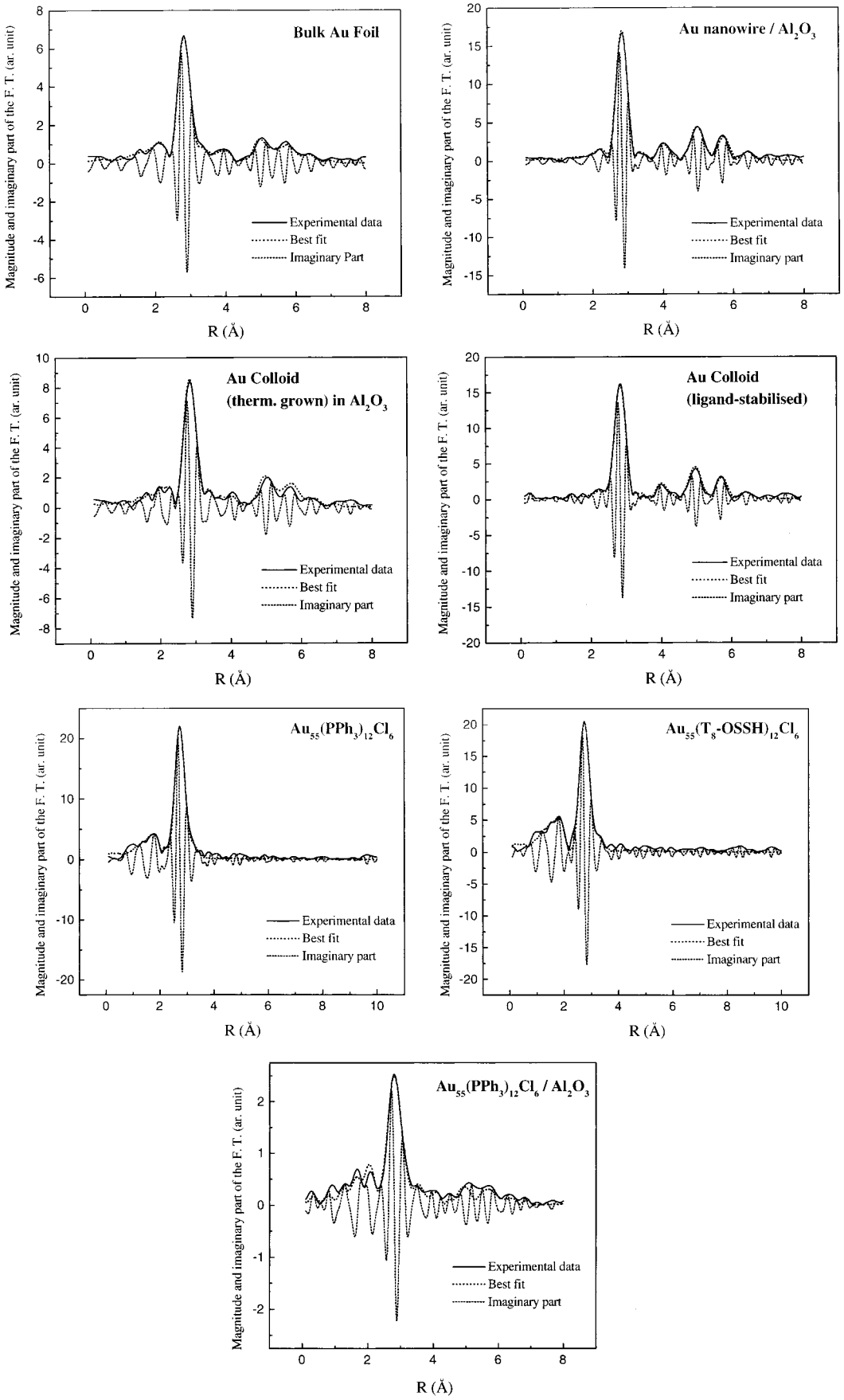

Figure 3. FTs of bulk gold and the series of gold nanomaterials. The solid lines are the experimental data, the thick dotted lines are the best fits, and the light dotted lines are the imaginary parts.

corresponding to the first shell has a very high magnitude and the Debye−Waller factor is exceptionally low. Peaks corresponding to outer-neighbor shells are also very marked (Figure 4). One interpretation of the low Debye−Waller factors could

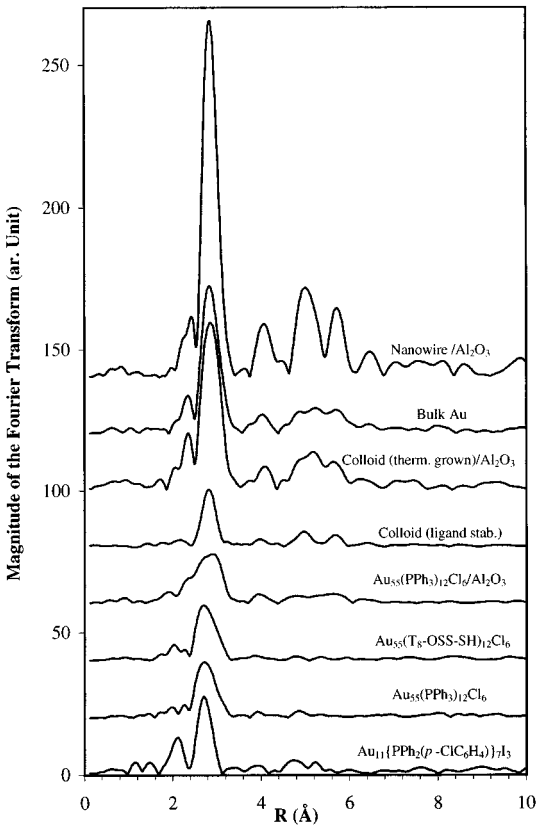

Figure 4. Fourier-transformed experimental Au L_3 edge of bulk gold and the series of gold nanomaterials. The FT of the Au_{11} ligand-stabilized cluster is presented as a reference.

be that the Au atoms are more tightly held in the nanowire than in bulk gold. However, this is not reflected in the Au−Au interatomic distances. We consider that a better explanation is that the gold nanowire sample has better crystallinity than the gold foil, for example, the relative absence of disorder in the form of stacking faults. This idea is supported by the WAXS study (see below). Additionally, EXAFS refinements of nanowires of silver and iron (in progress) show the same effect.[22] The ligand-stabilized gold colloids also had a low Debye−Waller factor, while the thermally grown colloids within the alumina had a Debye−Waller factor similar to the bulk value. In contrast, the high Debye−Waller factors reported for the two ligand-stabilized clusters showed the presence of a significant amount of structural disorder in these samples, as usually found for small metal cluster sizes.[23,24]

Apart from the lower coordination number of the ligand-stabilized colloid (8.6) due to its smaller size, the structure of these colloids was found to be similar to that of the bulk without exceptionally high peaks. Except for the ligand-stabilized clusters and colloid, the coordination numbers were not allowed to vary. In the case of the ligand-stabilized compounds, the coordination numbers of the two clusters $Au_{55}(PPh_3)_{12}Cl_6$ and $Au_{55}(T_{8-}OSS-SH)_{12}Cl_6$, 6.5 and 6.3, respectively, were substantially lower than for bulk Au, as expected from the presence of a high proportion[25] of surface atoms in the cluster. These values are slightly lower than expected (ideally 7.85) for a cubooctahedral cluster of 55 atoms[25] but are within the typical uncertainty on these factors.

There has been some controversy about the fcc structure of the Au_{55} clusters. Rapoport et al.[26] have found evidence of an icosahedral-based structure for the $Au_{55}(PPh_3)_{12}Cl_6$ cluster, using Debye function analysis of X-ray scattering data. This method, using ab initio numerical simulations, gives information regarding the size distribution and morphology of the metal atoms in a cluster.[27] It is important to recognize that the icosahedral structure requires a bimodal distribution of nearest-neighbor Au−Au distances,[21,28] amounting to a 0.2 Å splitting between the radial and tangential Au−Au distances. This structural model was tried during our fitting procedure of the two Au_{55} ligand-stabilized clusters, but the *R* factor for this model remained extremely high (at least 190%). Moreover, we can compare this analysis with that of the Au L_3 EXAFS of the cluster $Au_{11}\{PPh_2(p\text{-}ClC_6H_4)\}_7I_3$ (previously reported in ref 21, and now repeated with the improved potentials and phase shift corrections in EXCURV98). This cluster is known from crystallography to have a structure based on an icosahedron. Comparison of the EXAFS FT of $Au_{11}\{PPh_2(p\text{-}ClC_6H_4)\}_7I_3$ with those of the Au_{55} clusters showed that their shape was very different (Figure 4). The refinement of the Au_{55} cluster EXAFS data led to a very good agreement factor with only one metal coordination shell at 2.79 Å, consistent with a cubic close-packed geometry. On the other hand, a good refinement for the Au_{11} cluster was only obtained with a split metal first coordination shell with two contributions at 2.68 and 2.89 Å.

The existence of two very close shells in the Au_{11} cluster is also visible on its EXAFS spectrum with the presence of a beat. This study shows clearly that the Au_{11} and Au_{55} clusters feature two different structures and allows us to discard definitively the icosahedral model for the Au_{55} clusters. This conclusion is reinforced by the XANES analysis (see below) and by the WAXS measurement (see below).

An explanation must be sought for this discrepancy between our EXAFS analysis and the Debye function analysis of ref 26. The EXAFS data are dominated by individual nearest-neighbor Au−Au distances which conform to a regular cubic close-packed geometry. On the other hand, the X-ray scattering data depend on periodicity and so emphasize longer range Au−Au distances to a much greater degree. The surface layers in gold clusters of this size are likely to be distorted by the presence of the ligands. Indeed, as mentioned above, the magnitudes of the EXAFS Debye−Waller factors for the Au_{55} clusters are evidence for the presence of a structural disorder, as previously concluded for Pd clusters.[23] Additionally, the surface atoms in a small cluster will vibrate in an anharmonic potential, leading to asymmetric pair distribution functions, which will be emphasized for outer-neighbor distances. The X-ray scattering data of ref 26 were recorded at room temperature. So when the different physical bases of the EXAFS and X-ray scattering experiments are taken into account, the apparent disagreement can be resolved.

It is important to note that our EXAFS analysis does not prove whether the fcc gold clusters have a cubooctahedral overall shape. Other fcc geometries such as truncated octahedral forms would give identical EXAFS results.

XANES Analysis. *General Features*. XANES gives useful structural information such as the oxidation state of chemical species, site symmetry, and covalent bond strength, and it has widely been used to infer the local structure around the central atom. XANES is also suitable to investigate bound (local) empty states of unoccupied bands projected on the atom under study.[29,30]

Background-corrected and normalized experimental XANES Au L_3 spectra are shown in Figure 5. This figure also includes the XANES of the cluster[21] $Au_{11}\{PPh_2(p\text{-}ClC_6H_4)\}_7I_3$ and of two coordination compounds,[31] $KAuCl_4$ and $(PPh_3)AuCl$, as standard samples.

Four distinct near-edge features, A−D, can be pointed out

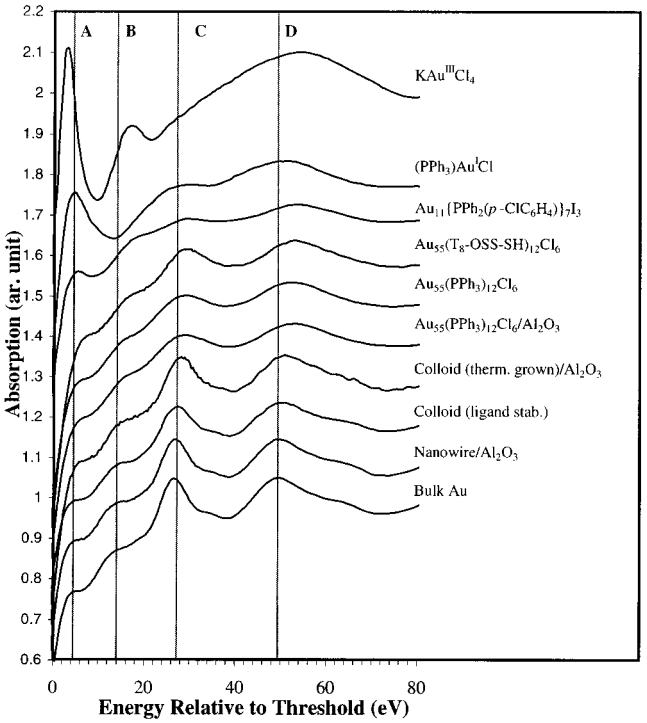

Figure 5. Au L_3 edge normalized XANES spectra of bulk gold, the series of gold nanomaterials, and reference compounds. The distinct features A−D are indicated in the plot.

in the first 60 eV past the edge. They are indicated in the plot (Figure 5). The peak located at 4 eV past the edge, labeled A, corresponds to the so-called "white line" characteristic of the transition metals. The reference compounds $KAu^{III}Cl_4$ and $(PPh_3)Au^{I}Cl$ with Au present in higher oxidation states[31] show clearly a strong increase of this peak. This feature is normally suppressed in the case of the bulk gold due to the nominally full occupancy of the d states (see below).

The presence of a small white line in $Au_{11}\{PPh_2(p\text{-}ClC_6H_4)\}_7I_3$ certainly means that Au in this cluster is slightly oxidized when compared to the bulk Au. This is consistent with a less metallic type of bonding than for larger clusters, the formal charge of +3 being distributed over 11 gold atoms. The Au_{55} clusters on the other hand have a much smaller white line, quantitatively resembling the bulk metal very closely, and consistent with a formal charge of +6 being delocalized over 55 Au atoms.

The other peaks, B−D, correspond to resonance features characteristic of the extended local structure around the absorbing atom. The peak at 15 eV past the edge (labeled B in Figure 5) is a weak feature but one which is consistently present in the bulk, nanowire, and colloidal samples, moving to slightly higher energies in the Au_{55} and Au_{11} clusters.

The peaks at 27 and 49 eV past the edge (C and D in Figure 5), belonging to the higher energy part of the XANES spectrum, are much more structure dependent. When the evolution of the C feature is observed according to the sample type, four different types of spectra can be pointed out.

The bulk gold and the nanowire show very similar C features. The shape of the two colloid spectra is also close to that of the bulk Au spectrum, but their C features have lower intensity. However, in the case of the thermally grown colloid within the alumina pores, the C peak is slightly shifted toward higher energies.

The spectra for the Au_{55} cluster deposited inside the alumina membrane and for the Au_{55} ligand-stabilized clusters show a broader and less intense C peak which is also shifted toward higher energies when compared to that of the bulk metal. In the spectrum for the Au_{11} cluster the C peak is almost completely absent.

According to the XANES feature concerned, a shift toward higher energies can be attributed to a smaller interatomic distance as well as an increased oxidation state of the metal.[32,33] In our case, the progressive shift toward higher energies observed for the C feature when going from the bulk metal, the nanowire, and the colloids to the cluster in the alumina and finally to the two ligand-stabilized Au_{55} clusters seems clearly linked to the constant decrease of the Au−Au distances found in the EXAFS study.

As a similar study on copper clusters showed,[34,35] the intensity and the width of these resonance peaks in the XANES part of the spectrum can also be related to the number of neighbors surrounding each gold atom and, more generally, to the size of the gold particle. In general, the more neighbors present the more intense and defined are these peaks (5−6 shells of atoms are required for the cluster to reproduce a XANES spectrum similar to that of bulk metal).[36] In our spectra this is consistent with the evolution of the environment of the gold atoms according to the type of sample.

Finally, the shape of the XANES spectrum of the icosahedral Au_{11} cluster shows features totally different from those of the two Au_{55} clusters, confirming once again the difference in the structural type of these two clusters.

$L_3 - kL_2$ Area Calculations. The X-ray absorption L_2 edge and L_3 edge correspond, respectively, to the transition of an electron from an initial core state 2p level to an empty final d state by X-ray photons. Since the spin−orbit splitting is important in the 5d band metals and according to the selection rule on l and j ($\Delta l = \pm 1$ and $\Delta j = 0, \pm 1$), the L_3 edge corresponds to the allowed transitions $2p_{3/2}$ to $5d_{3/2}$ and $5d_{5/2}$, whereas the L_2 edge corresponds only to the allowed transition $2p_{1/2}$ to $5d_{3/2}$.

Though the 5d bands in bulk Au are normally filled, and both Au L_3 and L_2 edges exhibit no white lines, Lytle[37] has shown that there exists a small white line at the Au L_3 edge in accord with the band calculation of Mattheiss et al.,[38] who showed that there are unoccupied density states of $d_{5/2}$ and $d_{3/2}$ character in the vicinity of the Fermi level due to some level of s−p−d hybridization. Consequently, the white line intensity cannot be explained only in terms of electron deficiency, but the size of the particle must also be taken into account.[29] Nonetheless, there are clear numerical trends in the XANES analysis, which give semiquantitative insight into the development of bonding in these gold cluster materials.

To estimate the variation in densities of unoccupied 5d states above the Fermi level in a series of samples, four types of methods comparing the intensity of the absorption edge (area under the peak) have been developed by different authors.

The first one consists of evaluating the difference area between spectra from pure metal and metal alloys.[19] However, this technique leads to uncertainties due to errors in the energy scale. The second method leads to an absolute determination of the electron vacancies by fitting the edge with a sum of a Lorentzian reflecting the unoccupied density of states and an arctangent function.[39,40] A third method developed by Mansour et al.[41] aims at determining f_d, the charge fractional change of the number of d band vacancies relative to a reference material. This method does not attempt to determine the total number of unoccupied states and is not very dependent on an accurate determination of the absolute areas. Finally the last method using

TABLE 2: Area Values of the Difference Spectra $L_3 - kL_2$ (Given as eV Times the Step) of Bulk Gold and the Series of Gold Nanomaterials[a]

sample	$L_3 - kL_2$	sample	$L_3 - kL_2$
$KAu^{III}Cl_4$	9.0(3)	Au nanowire/Al_2O_3	2.9(3)
$(PPh_3)Au^{I}Cl$	6.2(3)	$Au_{55}(T_8-OSS-SH)_{12}Cl_6$	2.7(3)
bulk gold	4.1(3)	$Au_{55}(PPh_3)_{12}Cl_6$	2.7(3)
Au colloid (thermally grown)/Al_2O_3	4.1(3)	$Au_{55}(PPh_3)Cl_6/Al_2O_3$	2.4(3)
Au colloid (ligand-stabilized)	3.8(3)		

[a] The area values of the Au_{11} ligand-stabilized cluster $KAu^{III}Cl_4$ and $(PPh_3)Au^{I}Cl$ are presented as references.

the normalized difference area ($L_3 - kL_2$) should provide a measurement of the variation of the electron vacancies in the $5d_{5/2}$ band of metals such as platinum[19] and gold.[38,41,42] This $L_3 - kL_2$ method minimizes the uncertainty, which arises from the calibration by using the EXAFS oscillations, and therefore appears to be the best procedure to extract reliable semiquantitative estimations.

Table 2 shows the results of the $L_3 - kL_2$ calculations for the gold cluster materials studied in this work and for some other reference materials. The results show a clear decreasing trend of the $L_3 - kL_2$ values from the highly oxidized samples to the ligand-stabilized Au_{55} clusters.

The high values found for the two compounds $KAu^{III}Cl_4$ and $(PPh_3)Au^{I}Cl$, 9 and 6.2, respectively, compared to 4.1 for the bulk metal suggest in this case that the intensity is certainly linked to an electron deficiency in the d orbital. The colloid grown thermally inside the membrane and the bulk have the same value of 4.1. The ligand-stabilized colloid has a slightly lower value of 3.8. These results point out the great similarity of these three samples.

At least two physical phenomena can affect the intensity of the white line: the size of the cluster, which can be considered as an intrinsic effect, and a possible charge transfer between the cluster and the support, which can be considered as an extrinsic one.[43] The small value of 2.7 found for both ligand-stabilized Au_{55} clusters could be linked to some charge transfer from the ligands, which is absent in the other cluster samples. However, if this effect were to dominate, we would expect significantly different values for these two compounds because of the differing σ-donor and π-acceptor character of the ligands. We therefore consider the small values of $L_3 - kL_2$ for these materials to arise predominantly from the small cluster size. The effect of the size of the particle on the $L_3 - kL_2$ value could be explained by a stronger d−d interaction in the small particles than in bulk metal.[36] This interaction, which favors a $s \rightarrow d$ rehybridization, reduces the d hole count and the value of $L_3 - kL_2$. This is consistent with the slightly compressed lattice found in the case of small clusters. On the contrary, $s \leftarrow d$ rehybridization in gold metal pushes a small amount of d character above the Fermi level, yielding an electronic configuration of $6s^{1+\delta},5d^{10-\delta}$ ($\delta \approx 0.1$ e).

The same value found for these two clusters confirms their great similarity in terms of electronic properties.

The smallest value in the series has been found for the Au_{55} cluster inside the alumina membrane with 2.4. This result may confirm a dual effect of the membrane and the size of the particle on the occupancy of the $d_{5/2}$ states. Finally, the low value of 2.9 found for the nanowire may result from some electron transfer from the membrane, but could also reflect the small size of the crystallites in this material. This would indicate that the electronic properties of the nanowire are closer to those of the Au_{55} clusters than to those of bulk gold. This is also consistent with the WAXS results showing that the nanowire is composed of small size crystallites (see below).

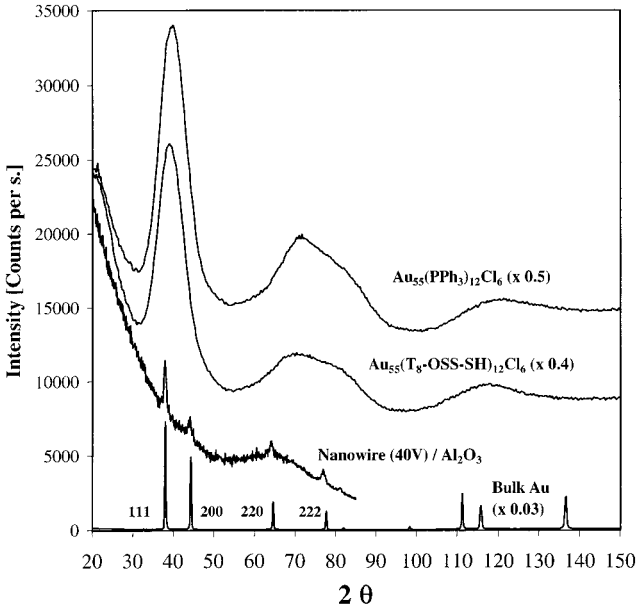

Figure 6. WAXS profiles of the two ligand-stabilized Au_{55} clusters and the gold nanowire in the 40 V alumina membrane. A gold foil profile is presented as a reference.

WAXS Analysis. Figure 6 shows the WAXS data of the two ligand-stabilized clusters $Au_{55}(PPh_3)_{12}Cl_6$ and $Au_{55}(T_8-OSS-SH)_{12}Cl_6$, the nanowire grown by electroplating in the 40 V alumina membrane, and a gold foil taken as a reference. In the case of the nanowire the X-ray beam was parallel to the pores. The pattern of the nanowire could be indexed with the fcc gold structure, but the peaks beyond the first one were found to be very weak at large angles. The pattern of the two clusters showed a broad peak around $2\theta = 39°$ corresponding mainly to the 111 reflection. This is a larger angle than for the bulk, confirming the shorter Au−Au distances in the clusters. However, due to the general poor definition of the peaks, the 111 peak also included to a small extent some contribution from the 200 reflection.

The WAXS gives further evidence for the geometries of these Au_{55} clusters. Simulations of X-ray diffraction patterns[44,45] have shown that icosahedral gold clusters would give rise to a clear additional feature around s ($= 2 \sin \theta/\lambda$) $= 5.5$ nm^{-1}, corresponding to a 2θ of 50°. This feature is completely absent in our experimental data (Figure 6), although it is visible in one of the X-ray scattering patterns reported in ref 26. The icosahedral structure can again be ruled out for our samples. However, the overall shape of the scattering pattern shows some characteristics of an amorphous long-range structure.[45,46] This may be caused by the distortion of outer-neighbor distances and the presence of some disorder as was shown by the EXAFS.

The cell parameters found from the WAXS analysis are presented in Table 3.

The results confirm that the Au−Au distances in the nanowire are almost identical to those in bulk gold, as also shown by the

TABLE 3: Values of the Mean Crystallite/Particle Diameter, Cell Parameters, and Au−Au First-Neighbor Bond Distances from the WAXS Data of Bulk Gold, the Gold Nanowire, and the Two Au_{55} Ligand-Stabilized Clusters[a]

sample	*t*	*a*	*R*
Au bulk metal		4.079	2.884
40 V Au nanowire	118.2	4.101	2.886
$Au_{55}(T_8{-}OSS{-}SH)_{12}Cl_6$	16.1	3.984	2.817
$Au_{55}(PPh_3)_{12}Cl_6$	11.4	3.924	2.775

[a] t = diameter of the crystallites (Å). a = cell parameter ($\lambda = 1.5315$ Å) (Å). R = smallest radial distance between two gold atoms (Å).

EXAFS. However, the WAXS results are systematically slightly longer than those from the EXAFS technique, even when considering that the EXAFS was done at 80 K while the WAXS measurements were taken at room temperature. This effect has often been observed, and is believed to arise from the cumulant fitting procedure used in EXAFS.[47]

The measurement of the fwhm of the peaks led to the crystallite diameters also presented in Table 3. In the case of the Au_{55} clusters the use of the Scherrer formula is more difficult because the diffraction peaks are not well enough defined. However, for the $Au_{55}(PPh_3)_{12}Cl_6$ cluster the size of 11.4 Å found using this method is in good agreement with the typical size expected for these clusters. On the other hand, the value of 16.1 Å found for the $Au_{55}(T_8{-}OSS{-}SH)_{12}Cl_6$ cluster indicates that some aggregation has occurred. A similar controlled aggregation was found on substitution of the PPh_3 ligands in $Au_{55}(PPh_3)_{12}Cl_6$ by amine ligands.[48] This aggregation could also explain the longer Au−Au distances (2.817 Å) than in the $Au_{55}(PPh_3)_{12}Cl_6$ (2.775 Å) sample found in this case.

The nanowires were found to have much larger particle size than the clusters, being composed on average of 120 Å crystallites.

A correlation between the size of the cluster or crystallite and the bond distance seems clear in this gold cluster system.

Conclusions

Metal nanowires, encapsulated within porous alumina membranes, represent a new class of one-dimensional "quantum wire". For them to find applications such as in electronic devices, a full characterization of their structures and electronic bonding is essential. This will enable their physical properties to be better understood. Our work has contributed to the achievement of these objectives by studying the structure and bonding of nanowires of gold, and comparing them with a series of gold cluster and colloid materials.

Clusters. The EXAFS, XANES, and WAXS analyses of both Au_{55} clusters confirm their fcc structure and the contraction of the lattice with the presence of metal−metal distances shorter than those of the bulk metal. The icosahedral structure previously suggested for $Au_{55}(PPh_3)_{12}Cl_6$ can definitively be ruled out.

The two Au_{55} clusters stabilized with different ligand shells, $Au_{55}(PPh_3)_{12}Cl_6$ and $Au_{55}(T_8{-}OSS{-}SH)_{12}Cl_6$, have closely similar structures and electronic properties. The exchange of ligands leads to slight aggregation of the gold clusters. Similarly, $Au_{55}(PPh_3)_{12}Cl_6$ undergoes slight aggregation when adsorbed into the alumina pores.

Colloids. The two colloids (one ligand-stabilized, the other grown thermally within the alumina membrane) are very similar with regard to structural and electronic properties to one another and also to the bulk metal. The lower number of nearest neighbors for the ligand-stabilized sample could indicate that the thermally grown colloids are of a bigger size.

Nanowires. The gold nanowires exhibit almost exactly the same structural features as bulk gold. However, the systematically much lower Debye−Waller factors associated with all the coordination shells in comparison to those of bulk gold, together with the intense peaks for outer-neighbor distances in the radial distribution function, suggest that the nanowires may have a much more ordered crystallinity than the corresponding metal foil. They were found to be composed on average of 120 Å crystallites. A smaller value of $L_3 - kL_2$ than for the bulk may be caused by some slight difference in the d band occupancy, suggesting that some electron transfer from the membrane may be the explanation. Alternatively, the effect may originate in the small crystallite size.

Our combined results show a clear pattern of buildup of metallic structure and bonding in these materials as the number of gold atoms increases. The structural characterization of these materials is an essential step to understanding their physical properties, which are being studied by the CLUPOS research network.[6]

Acknowledgment. For financial support we thank the EU TMR program, Contract Number FMRX-CT98-0177. We acknowledge the use of EPSRC's Chemical Database Service at Daresbury.[18]

References and Notes

(1) Schmid, G. *J. Chem. Soc., Dalton Trans.* **1998**, 1077.
(2) For a discussion see: Benfield, R. E.; Filipponi, A.; Morgante, N.; Schmid, G. *J. Organomet. Chem.* **1999**, *573*, 299.
(3) Thiel, R. C.; Benfield, R. E.; Zanoni, R.; Smit, H. H A.; Dirken, M. W.; *Struct. Bonding* **1993**, *81*, 1.
(4) de Jongh, L. J., Ed. *Physics and Chemistry of Metal Cluster Compounds*; Kluwer: Dordrecht, The Netherlands, 1994.
(5) Chen, S.; Ingram, R.; Hostetler, M.; Pietron, J.; Murray, R.; Schaaff, T.; Khoury, J.; Alvarez, M.; Whetten R. *Science* **1998**, *280*, 2098.
(6) EU TMR project "CLUPOS". Homepage: www.clupos.lth.se.
(7) Hornyak, G.; Kröll, M.; Pugin, R.; Sawitowski, T.; Schmid, G.; Bovin, J.-O.; Karsson, G.; Hofmeister, H.; Hopfe, S. *Chem. Eur. J.* **1997**, *3*, 1951.
(8) Hanaoka, T.-A.; Heilmann, A.; Kröll, M.; Kormann, H.-P.; Sawitowski, T.; Schmid, G.; Jutzi, P.; Klipp, A.; Kreibig, U.; Neuendorf, R. *Appl. Organomet. Chem.* **1998**, *12*, 367.
(9) Schmid, G. *Inorg. Synth.* **1990**, *7*, 214.
(10) Schmid, G.; Pugin, R.; Malm, J.-O.; Bovin, J.-O. *Eur. J. Inorg. Chem.* **1998**, *6*, 813.
(11) Schmid, G.; Lehnert, A. *Angew. Chem., Int. Ed. Engl.* **1989**, *28*, 780.
(12) Diggle, J. W.; Downie, T. C.; Goulding, C. W. *Chem. Rev.* **1996**, *69*, 365.
(13) Lohrengel, M. M. *Mater. Sci. Eng.* **1993**, *R11*, 243.
(14) O'Sullivan, J. P.; Wood, G. C. *Proc. R. Soc. London* **1970**, *A317*, 511.
(15) Foss, C. A.; Hornyak, G. L.; Stockert, J. A.; Martin, C. R. J. *Phys. Chem.* **1994**, *98*, 2963.
(16) Benfield, R. E.; Grandjean, D.; Dore, J. C.; Kröll, M.; Schmid, G.; Le Bolloc'h, D.; Kyotani, T. Manuscript in preparation.
(17) Binsted, N.; Campbell, J. W.; Gurman, S. J.; Stephenson, P. C. *EXAFS Analysis Programs*; Daresbury Laboratory: Warrington, U.K., 1991.
(18) Fletcher; D. A.; McMeeking, R. F.; Parkin, D. The United Kingdom Chemical Database Service. *J. Chem. Inf. Comput. Sci.* **1996**, *36*, 746.
(19) Moraweck, B.; Renouprez, A. J.; Hlil, E. K.; Baudoing-Savois, R. *J. Phys. Chem.* **1993**, *97*, 4288. Hlil, E. K.; Baudoing-Savois, R.; Moraweck, B.; Renouprez, A. J. *J. Phys. Chem.* **1996**, *100*, 3102.
(20) Neupert, V.; Peters, S.; Rey, V. *SPECPLOT*; ESRF: Grenoble, France, 1998.
(21) Cluskey, P. D.; Newport, R. J.; Benfield, R. E.; Gurman, S. J.; Schmid, G.; *Z. Phys.* **1993**, *D26*, S11.
(22) Benfield, R. E.; Grandjean, D.; Kröll, M.; Schmid, G. Manuscript in preparation.
(23) Benfield, R. E.; Filipponi, A.; Bowron, D. T.; Newport, R. J.; Gurman, S. J.; Schmid, G. *Physica B* **1995**, *208*, 671.
(24) Boyanov, B. I.; Morrison, T. I. *J. Phys. Chem.* **1996**, *100*, 16310.
(25) Benfield, R. E. *J. Chem. Soc., Faraday Trans.* **1992**, *88*, 1107.

(26) Rapoport, D. H.; Vogel, W.; Coelfen, H.; Schloegl, R. *J. Phys. Chem.* **1997**, *101*, 4175.
(27) Bazin, D. C.; Sayers, D. A., Rehr, J. J. *J. Phys. Chem. B* **1997**, *101*, 11040.
(28) Mackay, A. L. *Acta Crystallogr.* **1962**, *15*, 916.
(29) Prins, R.; Koningsberger, D. C. In *X-ray Absorption, Principles, Applications, Techniques of EXAFS, SEXAFS and XANES*; Koningsberger, D. C., Prins, R., Eds.; Wiley: New York, 1988; Chapter 8.
(30) Meitzner, G.; Via, G. H.; Lytle, F. W.; Sinfelt, J. H. *J. Phys. Chem.* **1992**, *96*, 4960.
(31) Benfield, R. E.; Filipponi, A.; Newport, R. J.; Bowron, D. T.; Gurman, S. J. *J. Phys.: Condens. Matter* **1994**, *41*, 8430.
(32) Bianconi, A. In *X-ray Absorption, Principles, Applications, Techniques of EXAFS, SEXAFS and XANES*; Koningsberger, D. C., Prins, R., Eds.; Wiley: New York, 1988; Chapter 11.
(33) Pandey, S. K.; Chetal, A. R. *Phys. Status Solidi* **1992**, *170*, 631.
(34) Greaves, G. N.; Durham, P. J.; Diakun, G.; Quinn, P. *Nature* **1981**, *294*, 139.
(35) Bazin, D.; Bensaddik, A.; Briois, V.; Sainctavit, Ph. *J. Phys. C4* **1996**, *6*, 481.
(36) Coulthard, L.; Degen, S.; Zhu, Y.-J.; Sham, T. K. *Can. J. Chem.* **1998**, *76*, 1707.
(37) Lytle, F. W.; Wei, P. S. P.; Greegor, R. B.; Via, G. H.; Sinfelt, J. H. *J. Chem. Phys.* **1979**, *70*, 4849.
(38) Mattheiss, L. F.; Dietz, R. E. *Phys. Rev.* **1980**, *B22*, 1663.
(39) Evans, J.; Mosselmans, J. F. W. *J. Phys. Chem.* **1991**, *95*, 9673.
(40) Behrens, P.; Assmann, S.; Bilow, U.; Linke, C.; Jansen, M. *Z. Anorg. Allg. Chem.* **1999**, *625*, 111.
(41) Mansour, A. N.; Cook, J. W., Jr.; Sayers, D. E. *J. Phys. Chem.* **1984**, *88*, 2330.
(42) Tyson, C. C.; Bzowski, A.; Kristof, P.; Kuhn, M.; Sammynaiken, R.; Sham, T. K. *Phys. Rev. B* **1992,** *45*, 8924.
(43) Bazin, D.; Sayers, D., Rehr, J. J., Mottet C. *J. Phys. Chem. B* **1997**, *101*, 5332.
(44) Cleveland, C. L.; Landman, U.; Schaaff, T. G.; Shafigullin, M. N.; Stephens, P. W.; Whetten, R. L. *Phys. Rev. Lett.* **1997**, *79*, 1873.
(45) Garzón, I. L.; Michaelian, K.; Beltrán, M. R.; Posada-Amarillas, A.; Ordejón, P.; Artacho, E.; Sánchez-Portal, D.; Soler, J. M. *Eur. Phys. J. D* **1999**, *9*, 211.
(46) Garzón, I. L.; Posada-Amarillas, A. *Phys. Rev. B* **1996**, *54*, 11796**.**
(47) Stern, E. A.; Ma, Y.; Hanske-Petitpierre, O.; Bouldin, C. E. *Phys. Rev. B* **1992**, *46*, 687**.**
(48) Brown, L. O.; Hutchison, J. E. *J. Am. Chem. Soc.* **1999**, *121*, 882.